Supporting information

The structural and mechanical properties of the *Orrorin tugenensis* femoral shaft and the assessment of bipedalism in early hominins*

Les propriétés structurales et mécaniques de la diaphyse fémorale de Orrorin tugenensis *et l'évaluation de la bipédie chez les hominines**

Laurent Puymerail [a,b†]

[a] *UMR 7268 CNRS–Université d'Aix-Marseille-EFS, Marseille, France*

[b] *UMR 7194 CNRS, Muséum national d'histoire naturelle, Paris, France*

Keywords: Femoral shaft; Outer morphology; Inner structure; Mechanical behaviour; Locomotion; Early hominins; *Orrorin tugenensis*

Mots clés: Diaphyse fémorale ; Morphologie externe ; Structure interne ; Comportement mécanique ; Locomotion ; Hominines anciens ; *Orrorin tugenensis*

* Note from the Associate Editors - This document, whose present format has been adapted by the AEs of this thematic issue, is the version available on 29 January 2014 (to R.M.) of an ongoing study developed by Dr. Laurent Puymerail on the structural morphology of the *Orrorin tugenensis* femoral shaft. Based on original research performed by the author during his PhD work (Puymerail, 2011), this unfinished document integrates written comments and text amendments to the early drafts provided by L. Bondioli (Rome), R. Macchiarelli (Poitiers, Paris) and P. O'Higgins (York), as well as some remarks from C.B. Ruff (Baltimore). At the time, comments on the early results of this study have been also provided by B. Senut (Paris). Based on the original CT record of the *Orrorin* specimens BAR 1002'00 and BAR 1003'00 kindly entrusted for study by B. Senut to L.P. and R.M., this document also benefited from comments provided to L.P. by L. Fitton (York), F. Marchal (Marseille), M. Pickford (Paris), B.G. Richmond (New York), M.J. Stock (Cambridge), V. Volpato (Frankfurt am Main) (and, very likely, by other colleagues as well). In its present version, this work does not include the discussion and the conclusions reached by L.P., both only developed in a preliminary format at the time of his untimely disappearance. In this respect, this ms. does not necessarily fully correspond to the views of the other colleagues having contributed the study and being supposed to co-author its final version (specifically, B.S., C.B.R., L.B., P.O.H., R.M.). We nonetheless opted for maintaining its form as close as possible to the original version. By rendering this valuable, but still incomplete work available in the scientific domain, we intend to share original results and encourage additional research on early hominin bone paleobiomechanics, notably on locomotory behaviours.

† Deceased 12 November 2015.

1. Introduction

Several features of postcranial skeletal anatomy indicate that early hominins combined arboreal and terrestrial locomotion with climbing, manifesting some degree of upright posture and enhanced facultative bipedalism (e.g., Lovejoy et al., 2009; Senut et al., 2001; Thorpe et al., 2007; Wood and Harrison, 2011). Key to interpreting fossil skeletal remains in terms of function and behaviour is the biomechanical characterization of bone gross and micro anatomy. Topographic variation in cross-sectional geometry and cortical bone distribution along the femoral shaft are expected to reflect the directions, frequencies, and magnitudes of habitual locomotor and postural loads (e.g., Morimoto et al., 2011a; Puymerail, 2013); in turn, how long bones mechanically respond to loads (load resistance) can be assessed using finite element analysis (e.g., Milne and O'Higgins, 2012).

Exploratory research aimed at comparatively assessing by 3D modelling the mechanical properties of the femoral shaft in *Homo*, *Pan* and *Gorilla* and at tentatively establishing how these relate to locomotion and phylogeny, identified two groupings: humans and African apes, where *Pan* is most similar to *Gorilla*, rather than its sister taxon, *Homo* (Puymerail, 2011, 2013; Puymerail and O'Higgins, 2013). Accordingly, we predicted that, given their inferred mixed arboreal-bipedal terrestrial locomotion, early hominin femora possess a distinctive functional signature.

Here we present the results of quantitative analyses that, for the first time, characterize the structural organization of cortical bone and mechanical behaviour of the femoral diaphysis in *Orrorin tugenensis*, a nearly 6.0 million year old (Sawada et al., 2002) basal member of the hominin clade (Senut et al., 2001) preserving postcranial evidence suggesting that its mosaic locomotor and positional repertoire likely associated some form of habitual terrestrial bipedal walking (but not in the exclusive or obligate sense of extant humans; Kuperavage et al., 2010) to movements in trees (Almécija et al., 2013; Bleuze, 2012; Galik et al., 2004; Gommery and Senut, 2006; Kuperavage and Eckhardt, 2009; Kuperavage et al., 2010; Lovejoy et al., 2009; Nakatsukasa et al., 2007; Pickford et al., 2002; Richmond and Jungers, 2008, 2012; Ruff and Higgins, 2013; Senut, 2006; Senut et al., 2001).

2. Materials and data collection

2.1. Orrorin tugenensis

The partial femurs BAR 1002'00 and BAR 1003'00 were collected on November 2000 at Kapsomin locality, Lukeino Formation, Kenya (Senut et al., 2001). BAR 1002'00, the most complete, represents the proximal two thirds of a left femur from a young adult individual; it lacks part of the greater trochanter but includes a complete head and an intact neck (even if originally

fractured). BAR 1003'00, which is larger and most robust compared to BAR 1002'00, is approximately the proximal half of a left femur preserving the entire lesser trochanter, but lacking the greater trochanter, most of the neck and the head. Estimated body weight for *Orrorin* from these femoral remains is 30 to 50 kg (Nakatsukasa et al., 2007).

In 2001 BAR 1002'00 and BAR 1003'00 were scanned at the Clinique Pasteur, Toulouse. Scans were obtained using a Marconi Twin Flash CT Scanner according to the following parameters: 120 kV and 100 mA, for BAR 1002'00, and 200 mA, for BAR 1003'00. The final volumes were reconstructed in DICOM format with a spatial resolution of 434 µm (*x* and *y*) and 1000 µm (*z*) for BAR 1002'00, and 250 µm (x and y) and 1000 µm (z) for BAR 1003'00 (Galik et al., 2004) (Fig. 1).

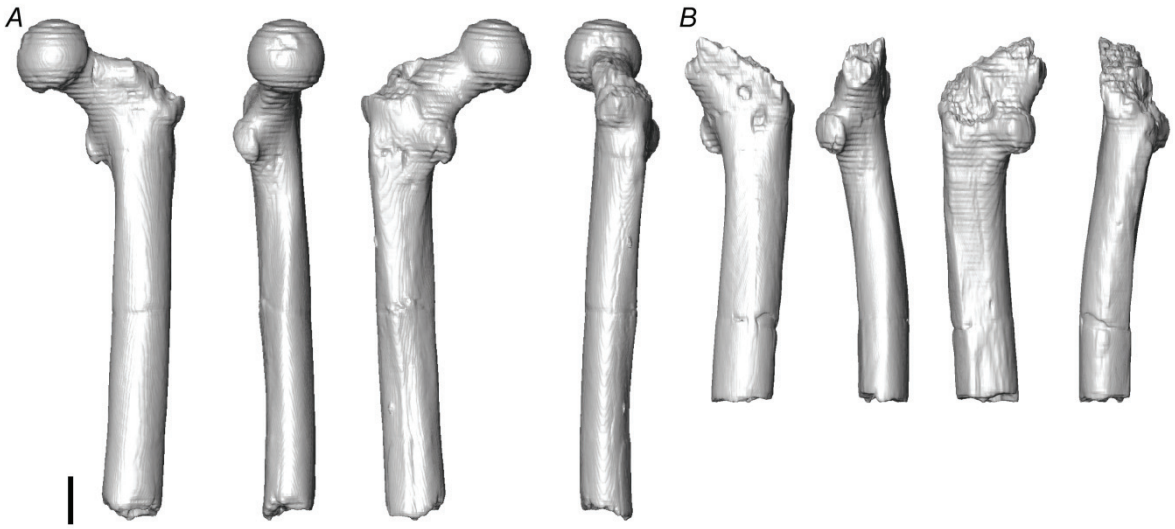

Fig. 1. CT-based 3D virtual reconstruction of the external aspects of BAR 1002'00 (A) and BAR 1003'00 (B) in (from left to right) anterior, medial, posterior, and lateral views. Scale bar, 2 cm.

Fig. 1. Reconstruction virtuelle 3D basée sur le registre CT des aspects externes de BAR 1002'00 (A) et BAR 1003'00 (B) en vues (de gauche à droite) antérieure, médiale, postérieure et latérale. Échelle, 2 cm.

With respect to the original pictures of BAR 1002'00 and BAR 1003'00 (e.g., Kuperavage and Eckhardt, 2009: 480; Nakatsukasa et al., 2007: 172; Pickford et al., 2002: 195; Senut et al., 2001: 141), here the vertical axis of both shafts has been tilted of 27° clockwise (Fig. 1).

Differently from BAR 1003'00, the medullary cavity of BAR 1002'00 is partially filled by a cemented matrix (Fig. 2A). In order to virtually isolate its cortical shell, a semi-automatic threshold-based segmentation with manual corrections was carried out following the half-maximum height method (Spoor et al., 1993) and the region of interest thresholding protocol (ROI-Tb; Fajardo et al., 2002) and by taking repeated measurements on different slices of the virtual stack (Coleman and Colbert, 2007) by the Avizo v.6.2. (Visualization Sciences Group Inc.) and ImageJ v.1.46a (Rasband, 2010) packages. Due to the similarity in Hounsfield values between cortical bone and

sediment filling at some local spots along this shaft and of a transversal fracture running midway between the lesser trochanter and the distal end, some interpolations of the medullary cavity outline have been realized (Fig. 2B). A similar procedure has also interested a few slices of BAR 1003'00 because of a fracture rim occurring towards its distal end.

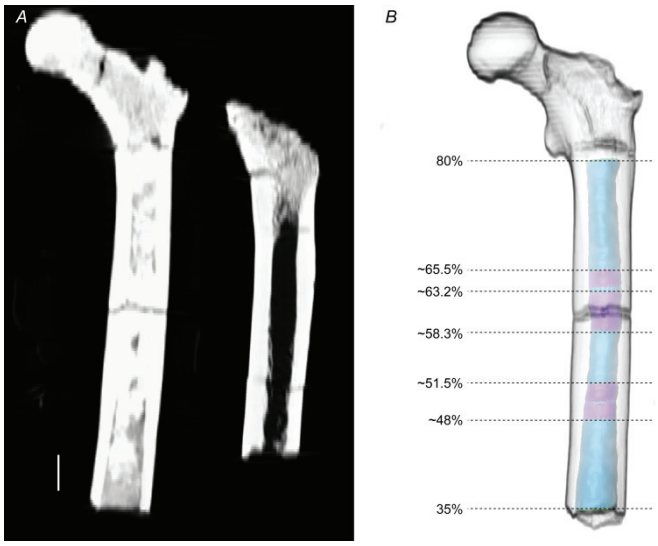

Fig. 2. (A) Coronal cross-sectional view of BAR 1002'00 (left) and BAR 1003'00 (right) revealing the sedimentary infill of BAR 1002'00. (B) 3D virtual reconstruction of BAR 1002'00 in semi-transparency showing the medullary filling (in cyan) and the interpolated medullary portions of the shaft (purple). Scale bar, 2 cm.

Fig. 2. Section longitudinale coronale de BAR 1002'00 (à gauche) and BAR 1003'00 (à droite) révélant le remplissage sédimentaire dans BAR 1002'00. (B) reconstruction virtuelle 3D de BAR 1002'00 en semi-transparence montrant le remplissage de la cavité médullaire (en cyan) et les portions de diaphyse interpolées (en violet). Échelle, 2 cm.

Based on the maximum femoral length estimation of 310 mm obtained for BAR1002'00 by Nakatsukasa and co-workers (2007) and by using the formula provided by McHenry (1974), we estimate the biomechanical length of this specimen as 287 mm. This sets the 80% section level about 12 mm below the distal edge of the lesser trochanter, an estimation which approximates the value of ca. 10 mm suggested by Ruff et al. (1999) for fossil hominin femora. The most distal section preserved for BAR 1002'00 is thus located at ~35% of the biomechanical length. For BAR 1003'00, we assume that the distal preserved section roughly corresponds to the midshaft (Nakatsukasa et al., 2007). Accordingly, the femoral biomechanical length is estimated at 297 mm. In combining these two estimations, the ~80% section is found 14 mm below the distal edge of the lesser trochanter. In all cases, our comparative structural analyses of the two specimens have considered the portion 50–80% (i.e. the proximal half) of the biomechanical length.

2.2. Comparative samples

We compared the results from BAR 1002'00 and BAR 1003'00 to similar evidence extracted from three adult samples (sexes pooled) of extant humans, chimpanzees and gorillas investigated according to the same protocols. The results, derived from taxa of known postural-locomotor behaviour, are used here to assess the extent to which biomechanical differences are evident between taxa and how these may relate to locomotion and phylogeny. In this comparative framework it is noteworthy that, in the extant hominid femoral shaft, the most discriminant information in terms of functionally-related endostructural organization (notably, cortical bone topographic distribution) is found within its proximal half (Puymerail, 2013).

The human sample (*Homo*) consists of 15 femora from as many individuals of both sexes (11 males, 2 females, and 2 of unknown sex) from Europe ($n = 9$), Central Africa ($n = 3$), North America ($n = 1$), and South America ($n = 2$) belonging to the historical osteological collections of the "Musée de l'Homme" of Paris, the University of Poitiers, and the Museo Nazionale Preistorico Etnografico "L. Pigorini" of Rome. *Pan troglodytes* is represented by 10 femora (3 males, 4 females and 3 individuals of unknown sex) selected from the African ape skeletal collections stored at the "Muséum national d'histoire naturelle" (MNHN) of Paris and the Senckenberg Forschungsinstitut und Naturmuseum of Frankfurt am Main (Puymerail, 2013). The gorilla (*Gorilla sp.*) sample consists of 9 femurs (6 males and 3 females) also selected from the primate osteological collections stored at the MNHN, Paris.

For the ape samples, detailed individual information about their original living environment (captive vs. wild) is not systematically available in the files. However, while Jensvold et al. (2001) noted that captive chimpanzees living in confined and less complex environments are characterized by lower locomotor activity, Marchi (2005, 2007) did not find significant differences between captive and wild apes in cross-sectional geometric properties of the tibia, fibula, hand and foot bones, a conclusion recently supported by Morimoto et al. (2011a) in their comparative morphometric mapping of the femoral shaft.

All extant human and ape femurs used for comparison with BAR 1002'00 and BAR 1003'00 have been selected because of their excellent preservation quality and absence of any alteration and/or gross pathology. The specimens have been scanned under standard conditions (Puymerail, 2011) using the medical CT equipment of four hospitals in France, Italy and Germany ($n = 31$) and the synchrotron radiation microtomographer (SR-μCT) set at the beamline ID 17 of the ESRF of Grenoble ($n = 3$). CT acquisitions resulted in voxel size ranging from 111 to 710 μm (for the x and y axes), and from 330 to 625 μm (for the z axis), while the SR-μCT acquisitions used an anisotropic voxel size of 350 μm.

3. Methods of analysis

Following their virtual cleaning and 3D outer and inner rendering based on CT-scans (Figs. 1, 2), we characterized the 50–80% portions of BAR 1002'00 and BAR 1003'00 for their morphology, cortical bone distribution and mechanical behaviour by coupling the results from four complementary analytical approaches: geometric morphometrics (GM) of the periosteal surface, morphometric maps (MMs) of cortical thickness distribution, cross-sectional geometry (CSG) and finite elements analysis (FEA).

3.1. Geometric morphometrics (GM)

Outer femoral shaft morphology does not only reflect functional biomechanical adaptation but is also constrained by other factors, including phylogeny and ontogeny (Morimoto et al., 2011b, 2012). Following the 3D GM analysis of the BAR 1002'00's proximal end (Almécija et al., 2013; for a classical morphometric analysis of the same specimen, see also Richmond and Jungers, 2008, 2012), here the periosteal surface of both *Orrorin*'s femoral diaphyses has been characterized by means of a regular mesh of 88 (semi)landmarks covering the portion 50-80% of the biomechanical length by using Amira v4.1.1 and Avizo v6.1 (Mercury Computer Systems, Inc.). These (semi)landmarks have no biological homology such as defined by Bookstein (1991), but biomechanical homology (O'Higgins et al., 2011, 2012; Oxnard and O'Higgins, 2009).

Deformation of the proximal part of the shaft was quantitatively assessed using GM approaches applied to the 3D coordinates of the 88 landmarks taken for each specimen from the unloaded and loaded models. These analyses based on landmark configuration or landmark displacement do not consider forces, energies or material properties, but lead to visual comparisons of deformation (Fitton et al., 2012; Milne and O'Higgins, 2012). From these different conformations, we performed a Procrustes superimposition (Generalized Procrustes Analysis) in the size and shape space (Bookstein, 1991; Dryden and Mardia, 1998; O'Higgins, 2000; Slice, 2005). Procrustes residuals were then considered and extracted from the unloaded case for each specimen. These residuals are next drawn onto the mean shape in order to facilitate visualization of the induced deformation and we put size back for each model according to relative centroid size (Fitton et al., 2012; Milne and O'Higgins, 2012; O'Higgins et al., 2011). Then, new landmarks coordinates from the unloaded mean and each individual load case were subject to generalized Procrustes analysis followed by principal components analysis. In a second time, analyses were conducted considering each individual by combining the three load cases for all individuals. Results are presented as principal component plots and deformations are visualized using a warped human proximal femoral shaft.

Morphologika² v.2.5. (O'Higgins and Jones, 2006) and EVAN toolbox v.1.62 were used for GM analysis.

3.2. Morphometric Maps (MMs)

Virtual cartography allows the bi-dimensional, planar representation of some local morphometric properties of a cylindrically-shaped three-dimensional object. The maps provide readily appraised, comprehensive representations of thickness distribution over entire objects and their use in the characterization and functional imaging of cortical bone topographic variation across the long bone shaft is a valuable tool in comparative structural and functional morphology (Bondoli et al., 2010; Zollikofer and Ponce de León, 2001). In order to synthetically reveal their structural signature (pattern), the periosteal surfaces of BAR 1002'00 and BAR 1003'00 have been mapped onto a cylinder (whose diameter corresponds to the maximum width of the vertical projection of the original outer surface of the shaft), virtually unzipped along a predefined vertical line along the anterior aspect, and then unrolled into a plane, where cortical bone topographic variation is rendered by a thickness-related colour scale (Bondioli et al., 2010; Morimoto et al., 2011a; Puymerail et al., 2012). For each point on the periosteal surface, site-specific bone thickness is defined here as the distance for each point from a node on the periosteal surface to its closest node on the endosteal surface (Bondioli et al., 2010; Mazurier et al., 2010). In the MMs, thickness values have been standardized between 0 and 1.

The evidence from the comparative hominid samples has been summarized into three taxon-specific consensus maps. In fact, since MMs have the same size and fully overlap, it is possible to perform generalized additive models (GAM) of interpolation to obtain consensus maps by merging sets of individual maps into a single dataset (Wood, 2006). Also, as the direction of unrolling changes according to the anatomical side of the investigated specimen, it is therefore possible to invert the polarity of this variable in order to obtain comparable maps, regardless the original sides. Accordingly, to allow a comprehensive visual comparison between the structural signature characterizing the *Orrorin* femora and the consensus maps summarizing the whole variation expressed by the comparative samples considered in this study, we used the pattern of relative thickness repartition (local morphometric properties) obtained by a custom routine developed in Scilab v.4.1.2 (The Scilab Consortium) with the support of the R v.2.11.1 (R Development Core Team, 2013) statistical software and the packages mgcv (Wood, 2006), spatstat (Baddeley, 2008), and gstat (Pebesma, 2004). We analysed the distribution of the individual maps by means of canonical variate analysis (CVA).

3.3. Cross-Sectional Geometry (CSG)

According to the "beam model" (Lovejoy et al., 1976; Ruff, 2008; Ruff and Hayes, 1983), certain geometric properties of the long bone diaphysis, which are considered as direct measures of mechanical characteristics, are determined at each cross-sectional level from the amount and site-specific distribution of material (here, cortical bone) (Lieberman et al., 2004; Ruff et al., 2006). As geometric section properties of the hominid hindlimb shafts predominantly reflect bending-related stresses during active locomotion, besides other canonical variables (see below), we focused on the percent of cortical area (%CA) and the cross-sectional shape index (I_x/I_y), since these ratios exclude direct size influence. The first parameter, which is a measure of strength (rigidity, or resistance) proportional to axial compressive and tensile strength, expresses the amount of cortical bone within each section, while the I_x/I_y ratio is an index of relative bending strength of the anteroposterior vs. mediolateral bone distribution (where ratios close to the unit reflect a nearly circular distribution of bone, while deviations reflect a more ovoid shape).

Cross-sectional geometric properties of the two *Orrorin* femora had been previously assessed at 35% (BAR 1002'00 only), 50%, 65% and 80% of the estimated biomechanical length (Bleuze, 2012; Kuperavage and Eckhardt, 2009), while here CSG properties have been measured in both BAR 1002'00 and BAR 1003'00 on virtual sections set at regular intervals of 1% along the entire 50-80% shaft portion (Table 1). The analyses were run by means of a custom routine developed in R v.2.11.1 (in Bondioli et al., 2010). Specifically, at each section we assessed: total area (TA, in mm^2); cortical area (CA, in mm^2); percent of cortical area (%CA); second moments of area about the anteroposterior (a-p) and the mediolateral (m-l) axes (I_x, I_y, in mm^4); polar second moment of area (J, in mm^4) (details in Ruff, 2008).

3.4. Finite Element Analysis (FEA)

FEA is commonly applied in studies of skeletal function to estimate the effects of loading and computing the resulting deformation and stress. In classical FEA studies, muscular constraints are simulated (Fitton et al., 2012; Viceconti et al., 2003). However, in our case, we compared the rheological responses of the proximal femoral shaft (50-80% portion) of fossil and extant hominid taxa representing different postural and locomotory modes and, most importantly, different (even unknown) muscular insertion patterns (Gibbs et al., 2000; Sigmon, 1974; Swindler and Wood, 1973). Accordingly, we uniquely modelled the non-physiological constraints and conventionally assumed isotropic bone material properties of 17 GPa for Young's modulus and 0.3 for Poisson's ratio (Carter and Beaupré, 2007; Currey, 2002; Reilly and Burstein, 1975). The models were constrained in all three directions at the distal cross-section (midshaft) by firstly simulating pure compression at the upper surface of the proximal section (80%) by applying a 10 N vector directed

toward the centre of the constrained midshaft section, then posterior bending and medial bending orthogonal to the major axis from the centre of the proximal section towards the posterior and the medial aspects, respectively (Fig. 3). In the results, where discrimination among the individuals is exclusively due to the magnitude, location and orientation of the induced displacements, two specimens close in the morphospace defined by a principal component axis are considered to share similar biomechanically-related characteristics, i.e. rheological and endostructural properties.

The 3D volume data of the periosteal and endosteal surfaces of BAR 1002'00 and BAR 1003'00 were exported as a stack of bitmap images and then converted into a linear brick FE meshes consisting of million eight-noded cubic elements using custom software. The analyses were performed using the software *VOX-FE* (Fagan et al., 2007).

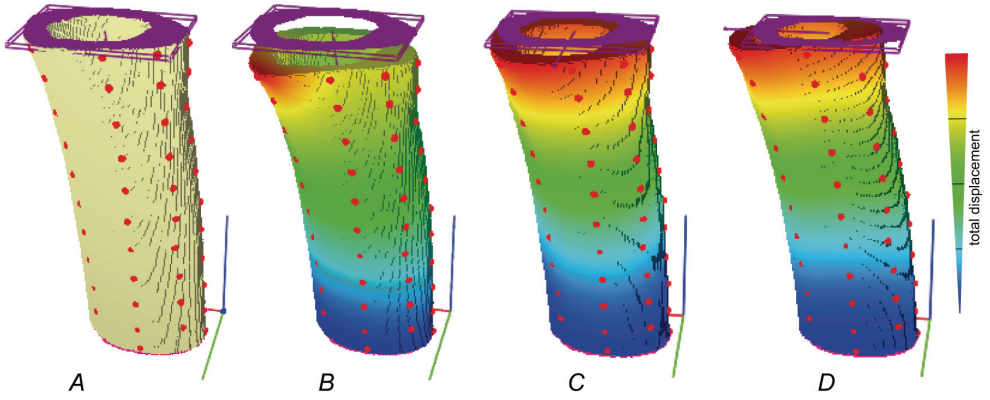

Fig. 3. Representation of the deformations of the femoral diaphysis (50-80% portion) of a gorilla according to different simulations. Original unloaded model (A) and results after modelling compression (B), posterior bending (C) and medial bending (D). Total displacement is represented by a colour-scale ranging from blue (no displacement) to red (maximum displacement). The red dots correspond to (semi)landmarks defining the shape of the diaphysis.

Fig. 3. Représentation des déformations de la diaphyse fémorale (portion entre 50 et 80%) d'un gorille en fonction de plusieurs simulations. Modèle original non contraint (A) et résultats après modélisations de compression (B), de torsion postérieure (C) et de torsion médiale (D). Le déplacement total est représenté par une échelle de couleur allant du bleu (aucun déplacement) au rouge (déplacement maximum). Les points rouges correspondent aux (semi)landmarks définissant la conformation de la diaphyse.

4. Results

4.1. Geometric morphometrics (GM)

The outer morphology of the extant human adult femoral diaphysis is unambiguously distinguished from that of the African apes by the first principal component of the Procrustes shape coordinates (PC1 = 80.7% of total variance) (Fig. 4). Because of an absolutely and relatively longer shaft, the human condition is characterized by negative values along the PC1, while *Pan* and *Gorilla*, with their shorter but larger shafts, by positive values. In this context, BAR 1002'00 is

found within the variation displayed by the chimp sample used in this study, while BAR 1003'00 falls among the humans.

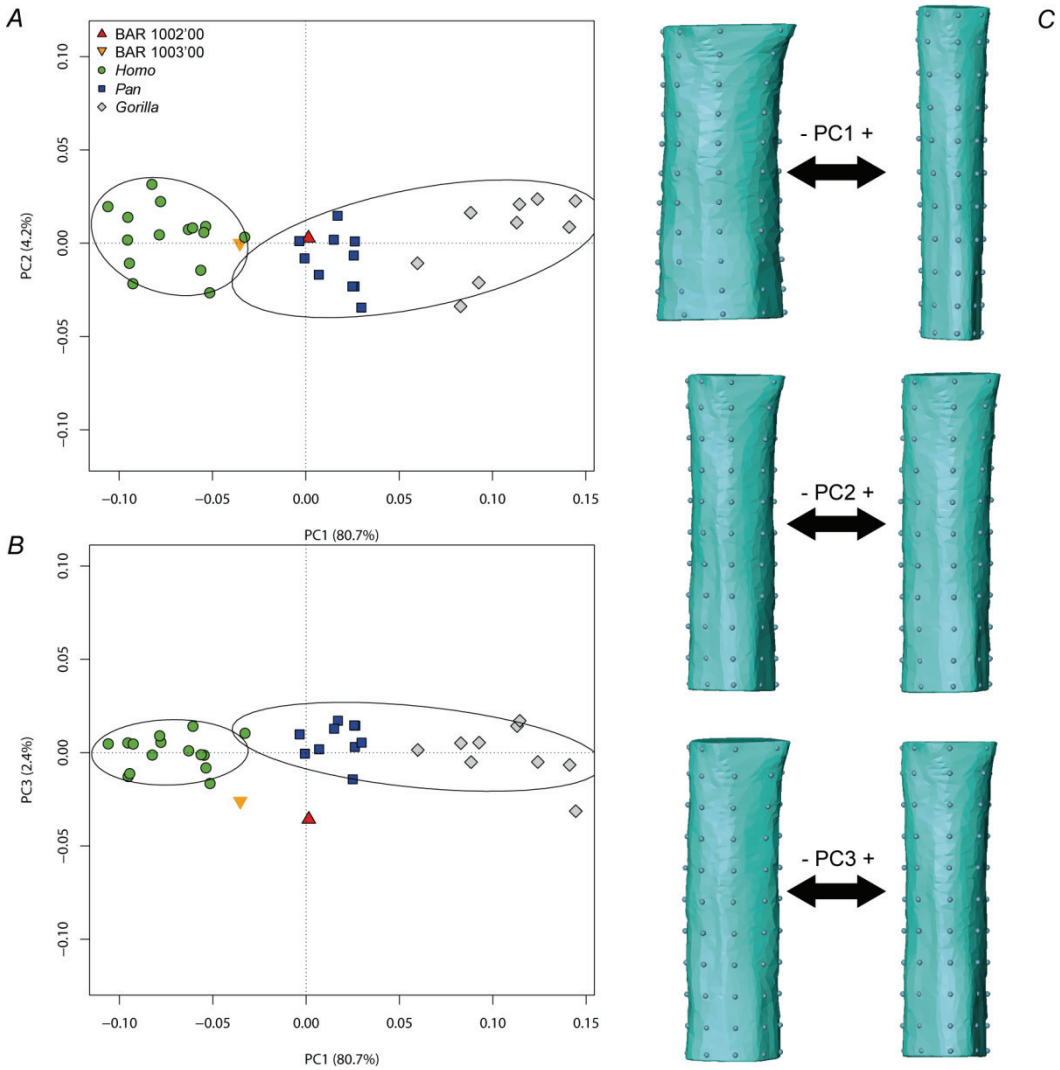

Fig. 4. Principal component scores (A: PC1 and PC2; B: PC1 and PC3) for Procrustes-registered coordinates of the femoral shaft periosteal surfaces (portion 50–80% of the biomechanical length) of BAR 1002'00 and BAR 1003'00 (*Orrorin*) and of three samples of extant humans (*Homo*), chimpanzees (*Pan*) and gorillas (*Gorilla*). (C) Warped external surfaces (based on thin-plate spline) representations of the investigated shaft portion in posterior view according to the extreme configurations along PC1, PC2 and PC3.

Fig. 4. Analyses en composantes principales (A : PC1 et PC2 ; B : PC1 et PC3) des coordonnées Procuste de la surface périostéale de la diaphyse fémorale (portion entre 50 et 80% de la longueur biomécanique) de BAR1002'00 et BAR1003'00 (*Orrorin*), ainsi que de trois échantillons actuels d'humains (*Homo*), chimpanzés (*Pan*) et gorilles (*Gorilla*). (C) surfaces externes déformées (basées sur des *thin-plate splines*) représentant la portion de diaphyse étudiée en vue postérieure des conformations extrêmes selon PC1, PC2 et PC3.

In order to estimate if allometry could explain this distribution pattern, we plotted the score of the first axis against the centroid size (CS) values of the corresponding specimens. Results indicate no correlation in humans ($R^2 = 0.01$, $p = 0.68$) but in great apes ($R^2 = 0.57$, $p = 0.001$), the young adult *Orrorin* specimen again falling within the chimp variation for CS, while BAR 1003'00 occupies an intermediate position between *Homo* and *Pan* (Fig. 5).

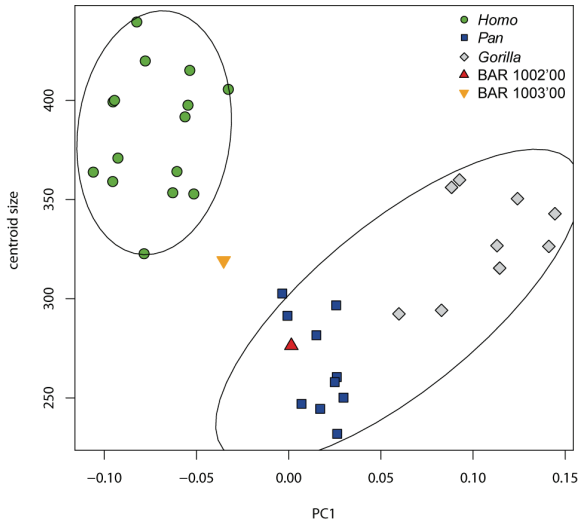

Fig. 5. Principal component score of the first axis (PC1) against centroid size of BAR1002'00 and BAR1003'00 (*Orrorin*), and of three samples of extant humans (*Homo*), chimpanzees (*Pan*) and gorillas (*Gorilla*) periosteal surfaces. The ellipse confidence interval is of 95%.

Fig. 5. Composantes principales du premier axe (PC1) en fonction de la taille centroïde de la surface périostéale de BAR1002'00 et BAR1003'00 (*Orrorin*), ainsi que de trois échantillons actuels d'humains (*Homo*), chimpanzés (*Pan*) et gorilles (*Gorilla*). L'intervalle de confiance de l'ellipse est de 95%.

4.2. Morphometric Maps (MMs)

The standardized maps revealing cortical bone thickness topographic distribution across the proximal femoral shaft in *Orrorin*, extant humans and the African apes are shown in Fig. 6. The structural signature displayed by the human consensus map features three major shaft reinforcements. The most developed corresponds to the posterior pilaster, where the thickest bone is found around the midshaft (Puymerail, 2011). Additional strengthening is recognizable at the level of the proximal lateral and medial aspects, the latter representing the structural continuity of the typical asymmetry in cortical bone thickness characterizing the configuration of the derived hominin femoral neck (Lovejoy et al., 2002; Matsumura et al., 2002; Ohman et al., 1997; Zebaze et al., 2005, 2007), a condition which has been also observed in *Orrorin* (Galik et al., 2004). However, while the posterior and medial features are systematically well expressed in the human femora, the degree of development of the lateral thickening is highly variable (Bondioli et al., 2010; Puymerail et al., 2012). This feature consists of two components. Its most distal portion, which is rather anteriorly oriented, is mostly found between 50% and 65% of the biomechanical length, while its proximal portion, between 65% and 80%, is oriented towards the posterior aspect. Together, these structural components roughly correspond to the outer attachment site of the *gluteus maximus* muscle (Carlson, 2006; Morimoto et al., 2011b; Sigmon, 1974; Swindler and Wood, 1973). Differently from *Homo*, in both African apes two reinforcements can be identified medially and laterally (Morimoto et al., 2011a; Puymerail, 2013). The former is the most extended, as it covers

the entire medial aspect of the proximal shaft, approximately between 40% and 80% of the biomechanical length (Puymerail, 2013). The lateral one, which is more proximally restricted (70-80%) and which in *Pan* corresponds on the external surface to the lateral spiral pilaster (Morimoto et al., 2011b), appears as a crook-shaped imprint (Puymerail, 2013). Finally, a variably developed posterior bone thickening is occasionally detected in *Pan* between 55% and 65% of the biomechanical length. While expressed with a different intensity because of their likely different taphonomic and diagenetic history, the *Orrorin*'s shafts present a similar pattern globally resembling the extant African ape structural signature. It essentially consists of an extended medial reinforcement and of a more proximally-set crooked-shaped lateral thickening.

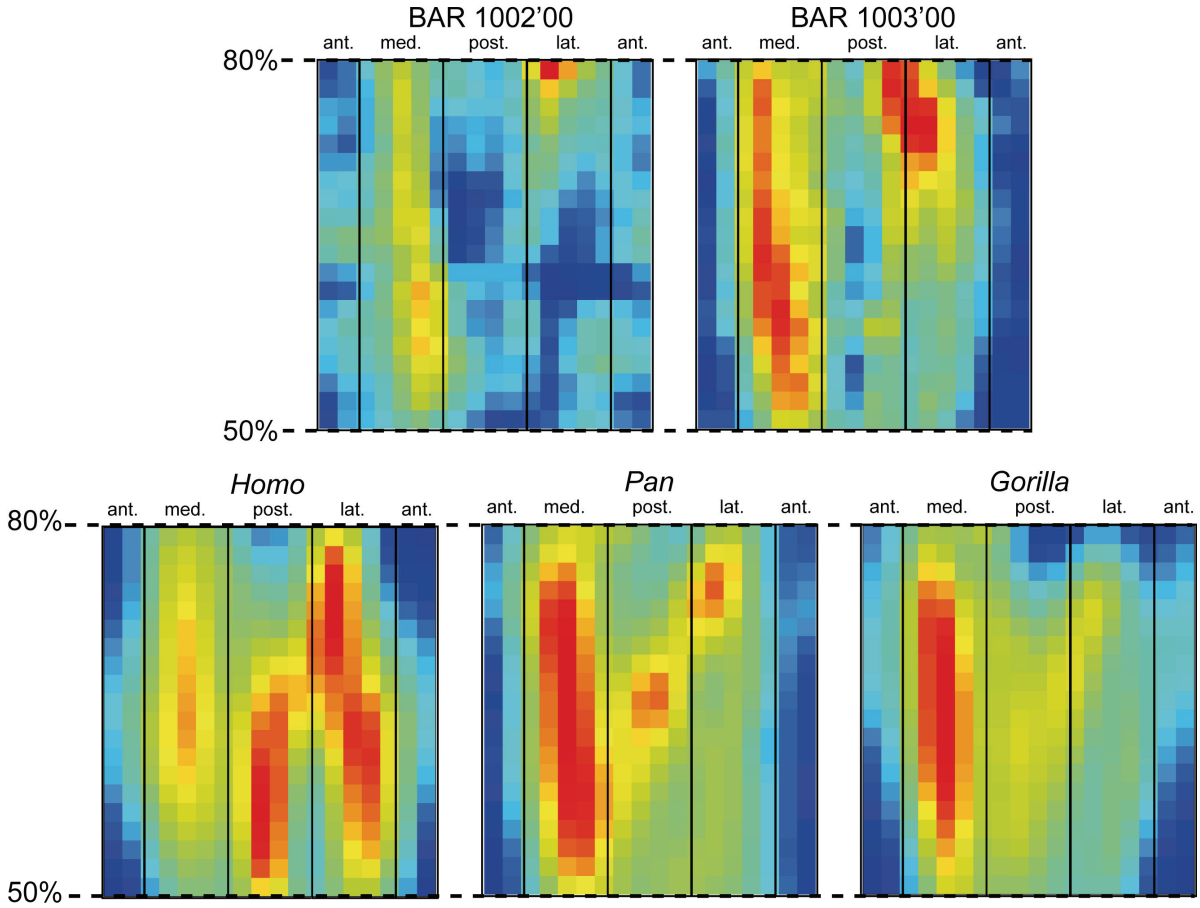

Fig. 6. Standardized morphometric maps of cortical bone thickness topographic variation along the femoral shaft (50–80% portion) in BAR 1002'00 and BAR 1003'00 (*Orrorin*) (individual maps) compared to the taxon-specific consensus maps obtained from three samples of extant humans (*Homo*), chimpanzees (*Pan*) and gorillas (*Gorilla*). All femora have been virtually unzipped vertically along the middle of their anterior aspect and then unrolled. Independently from the original side of the investigated specimens/samples, each map virtually represents a left femoral shaft. Imaging perspective is from the inner to the outer surface (medial is to the left). The maps are set within a grid of 18 columns (*x*) and 20 rows (*y*). Relative cortical thickness is rendered by a chromatic scale increasing from dark blue (0) to red (1). ant.: anterior; lat.: lateral; med.: medial; post.: posterior.

Fig. 6. Cartographies morphométriques standardisées de la variation d'épaisseur de l'os cortical le long de la diaphyse fémorale (portion entre 50–80%) pour BAR1002'00 et BAR1003'00 (*Orrorin*) comparées aux cartographies consensus propres aux taxons comparatifs incluant les humains actuels (*Homo*), les chimpanzés (*Pan*) et les gorilles (*Gorilla*). Tous les fémurs ont été déroulés virtuellement le long de leur aspect antérieur. Indépendamment de l'orientation originale des spécimens/échantillons inclus ici, chaque cartographie représente une diaphyse fémorale gauche. Le calcul

a été effectué de la surface interne vers celle externe (l'aspect médial est à gauche). Les cartes sont formées par une grille de 18 colonnes (*x*) et 20 lignes (*y*). L'épaisseur relative de l'os cortical est visualisée par une échelle chromatique allant du bleu (0) au rouge (1). ant. : antérieur ; lat. : latéral ; med. : médial; post. : postérieur.

Intra-taxic structural variation and the extent of inter-taxic similarities/differences in cortical bone thickness repartition assessed by canonical variate analysis (CVA) show that all human femora are well separated from those of *Gorilla*, *Pan* and *Orrorin* by the first canonical axis, while *Gorilla* and *Pan* are separated each other following the second axis, which also divides *Orrorin* from *Gorilla* (Fig. 7). With this respect, there is no misclassification among the extant specimens and both *Orrorin* femora are predicted to fall among the chimpanzees with an a posteriori probability of 0.99.

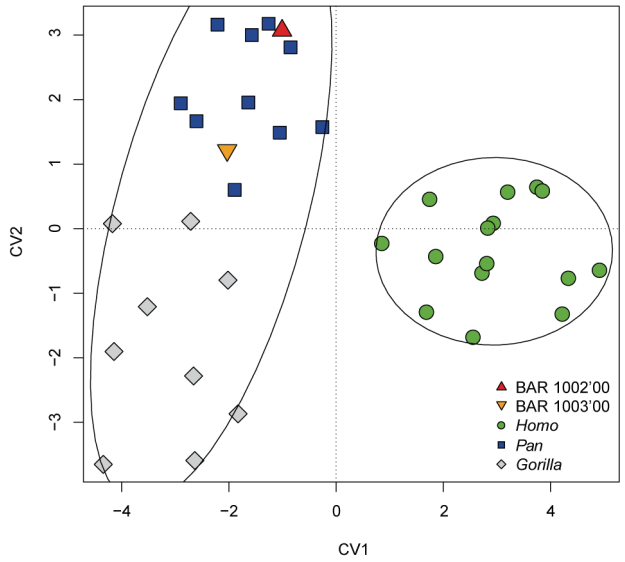

Fig. 7. Canonical variate analysis (CVA) of cortical thickness distribution as revealed by individual MMs of BAR1002'00 and BAR1003'00 (*Orrorin*) and of three samples of extant humans (*Homo*), chimpanzees (*Pan*) and gorillas (*Gorilla*) following the first and second axes. The ellipse confidence interval is of 95%.

Fig. 7. Analyse canonique (CVA) de la distribution d'épaisseur corticale issues des MMs individuelles de BAR1002'00 et BAR1003'00 (*Orrorin*), ainsi que de trois échantillons actuels d'humains (*Homo*), chimpanzés (*Pan*) et gorilles (*Gorilla*) selon le premier et deuxième axe. L'intervalle de confiance de l'ellipse est de 95%.

4.3. Cross-Sectional Geometry (CSG)

The values of the cross-sectional geometric properties measured (from distal to proximal) at 35%, 50%, 65%, and 80% of the biomechanical length in BAR 1002'00 and BAR 1003'00 (the latter, not at 35%) and in three comparative samples of extant humans, chimpanzees and gorillas are shown in Table 1.

Table 1

Selected values of the unstandardized cross-sectional geometric properties measured at 35%, 50%, 65% and 80% of the biomechanical length along the shaft in BAR 1002'00 and BAR 1003'00 (*Orrorin*) and three samples of extant humans (*Homo*), chimpanzees (*Pan*) and gorillas (*Gorilla*). For the comparative samples, the means and standard deviations (in italics) are provided. TA: total area (in mm^2); CA: cortical area (in mm^2); %CA: percent of cortical area; I_x, I_y, second moments of area about the anteroposterior and mediolateral axes (in mm^4); J, polar second moment of area (in mm^4).

Tableau 1

Valeurs sélectionnées des propriétés de géométrie de section non standardisées mesurées à intervalles réguliers (1%) le long de la portion de diaphyse fémorale comprise entre le 50^e (distal) et le 80^e (proximal) centile de la longueur biomécanique de BAR1002'00 et BAR1003'00 (*Orrorin*), ainsi que de trois échantillons actuels d'humains (*Homo*), chimpanzés (*Pan*) et gorilles (*Gorilla*) Pour les échantillons comparatifs, la moyenne et l'écart type (en italique) sont donnés. TA: aire totale (en mm^2) ; CA : aire corticale (en mm^2) ; %CA : pourcentage d'aire corticale ; I_x, I_y : seconds moments d'aire des axes antéropostérieur et mediolateral (en mm^4) ; *J* : second moment polaire de l'aire (en mm^4).

	spec./sample	TA	CA	%CA	I_x	I_y	J
35%	BAR 1002'00	464.2	261	56.2	12030.5	16093	28123
	Homo	591.7	352.5	59.3	22690	25290	48690
		130.9	*61.2*	*6.5*	*10264*	*9893*	*19955*
	Pan	390.8	233	59.9	10370	11500	20580
		68.1	*47.6*	*5.7*	*3571*	*4580*	*7757*
	Gorilla	910.2	567.6	59.1	40090	92970	130700
		181	*99.3*	*4.9*	*16766*	*25707*	*41511*
50%	BAR 1002'00	412.7	298.1	72.2	10409	15113	25523
	BAR 1003'00	443.4	324.7	73.2	12516	17525	30041
	Homo	525.4	403.7	75.5	24120	20730	43690
		107.5	*77.3*	*3.6*	*10668*	*8313*	*18694*
	Pan	407.6	254.3	63.3	11190	12410	22800
		72.5	*57.3*	*7.6*	*3974*	*4950*	*8596*
	Gorilla	939	631.5	70	45560	89040	137800
		182.6	*140.5*	*3.9*	*20638*	*27608*	*47500*
65%	BAR 1002'00	429.3	317.3	73.9	12203	15573	27777
	BAR 1003'00	455.4	339.7	74.6	13525	18700	32226
	Homo	525.7	431.3	80.6	22080	22630	43660
		120.4	*85.6*	*5.6*	*11127*	*9964*	*20355*
	Pan	411.3	260.5	66.1	11170	12080	22640
		72.4	*60.6*	*8.3*	*3998*	*5069*	*8846*
	Gorilla	969.5	677.5	74	57950	84540	142500
		184.8	*162.8*	*4.9*	*24216*	*26357*	*50177*
80%	BAR 1002'00	454.4	351.6	77.4	12862	19984	32847
	BAR 1003'00	472.9	363.3	76.8	15635	19539	35175
	Homo	581.4	417.2	71.8	20400	33300	53700
		149.2	*86.5*	*8.2*	*11829*	*14385*	*25672*
	Pan	436.2	260.6	62.7	11870	13080	24950
		77.9	*58.6*	*6.9*	*4682*	*5201*	*9783*
	Gorilla	1032	676.4	65.1	68180	96290	155900
		183.1	*170.6*	*8.4*	*23636*	*31391*	*54316*

In both *Orrorin* femora, percent of cortical area (%CA) slightly increases proximally, while the profile variably decreases within the shaft portion 65–80% of the biomechanical length in all three comparative modern hominid taxa, humans displaying the most curved outline (Fig. 8A). *Orrorin*'s values are intermediate between those of the relatively thicker *Homo* and thinner *Pan*, and more closely fit the *Gorilla* pattern, notably for the portion 50–70%. For the I_x/I_y shape ratio, *Orrorin* femora systematically display values below the unit, a condition shared with *Pan* and *Gorilla*, but not with modern humans, the latter showing the highest values, thus a proportionally higher strength to anteroposterior bending loads below 65% of the biomechanical length (Fig. 8B). Again, the closest fit to BAR 1002'00 and BAR 1003'00 is the *Gorilla*'s pattern. However, while *Orrorin*, *Gorilla*, *Pan*, and *Homo* are distinguishable for their biomechanical properties towards the midshaft, a predominant rigidity against mediolateral bending loads is universally found proximally.

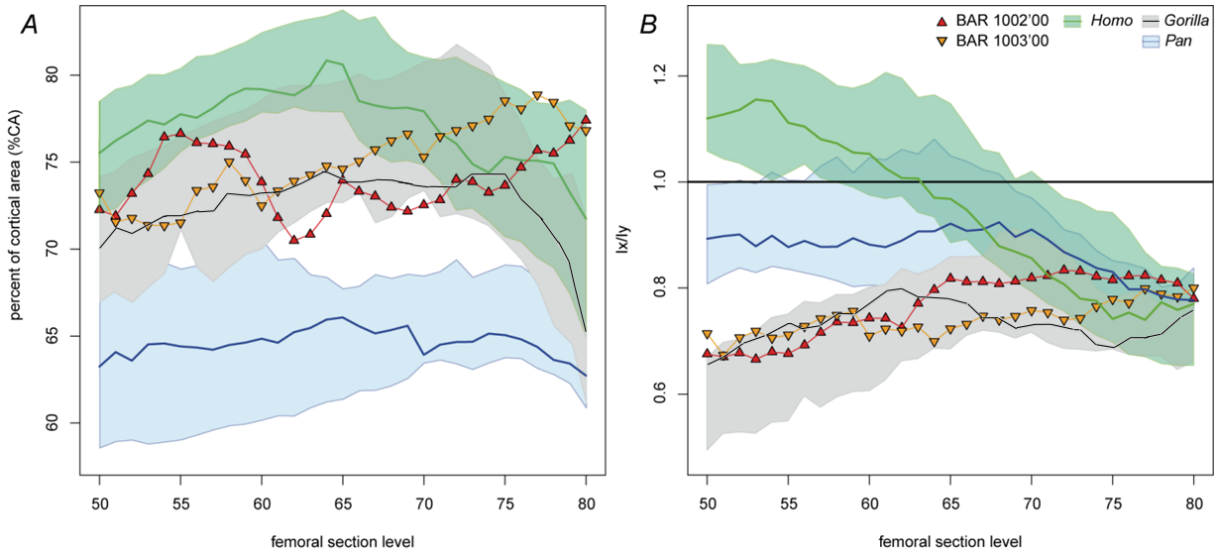

Fig. 8. Percent cortical area (A) and I_x/I_y shape ratio (B) measured at regular intervals of 1% along the femoral shaft portion comprised between 50% (distal) and 80% (proximal) of the biomechanical length in BAR 1002'00 and BAR 1003'00 (*Orrorin*) and three samples of extant humans (*Homo*), chimpanzees (*Pan*) and gorillas (*Gorilla*). For the comparative samples, the median and the interval between the first (Q1) and third (Q3) quartiles are provided.

Fig. 8. Pourcentage d'aire corticale (A) et rapport de forme (B) mesurés à intervalles réguliers de 1% le long de la portion de diaphyse fémorale comprise entre 50% (distal) et 80% (proximal) de la longueur biomécanique de BAR1002'00 et BAR1003'00 (*Orrorin*), ainsi que de trois échantillons actuels d'humains (*Homo*), chimpanzés (*Pan*) et gorilles (*Gorilla*) Pour les échantillons comparatifs, la médiane et l'intervalle entre le premier quartile (Q1) et le troisième quartile (Q3) sont représentés.

4.4. Finite Element Analysis (FEA)

In the bivariate plot for PC1 (67.4%) and PC2 (22.3%) of the individual load cases resulting from compression, posterior bending and medial bending (Fig. 9A), the gorillas predictably show the absolutely least deformed shafts, followed by chimp and finally by extant humans, the latter also showing the greatest variation for all directional constraints. Starting from the unloaded mean

specimen (black star), all medial bending simulations are characterized by negative values for PC1. The *Orrorin* femora, which are very close each other and quite far from *Gorilla*, fall within a morphospace where chimpanzees and humans overlap, even if *Homo* globally shows more negative scores. Conversely, all simulations for posterior bending present positive values on PC1. As seen for medial bending, gorillas present the lowest deformation and are relatively distinct (but one case). Here again, *Pan* and *Homo* overlap. While BAR 1002'00 falls within a *Pan-Homo* virtual space, BAR 1003'00 more closely fits the human pattern. The results of the simulations for compression basically overlap those from posterior bending on PC2, while they are clearly separated by PC3 (7.7%; Fig. 9B). Gorillas again show the least deformed shaft, followed by *Pan* and then *Homo*. For resistance to deformation, BAR 1002'00 falls between the African apes and BAR 1003'00 between *Pan* and *Homo*.

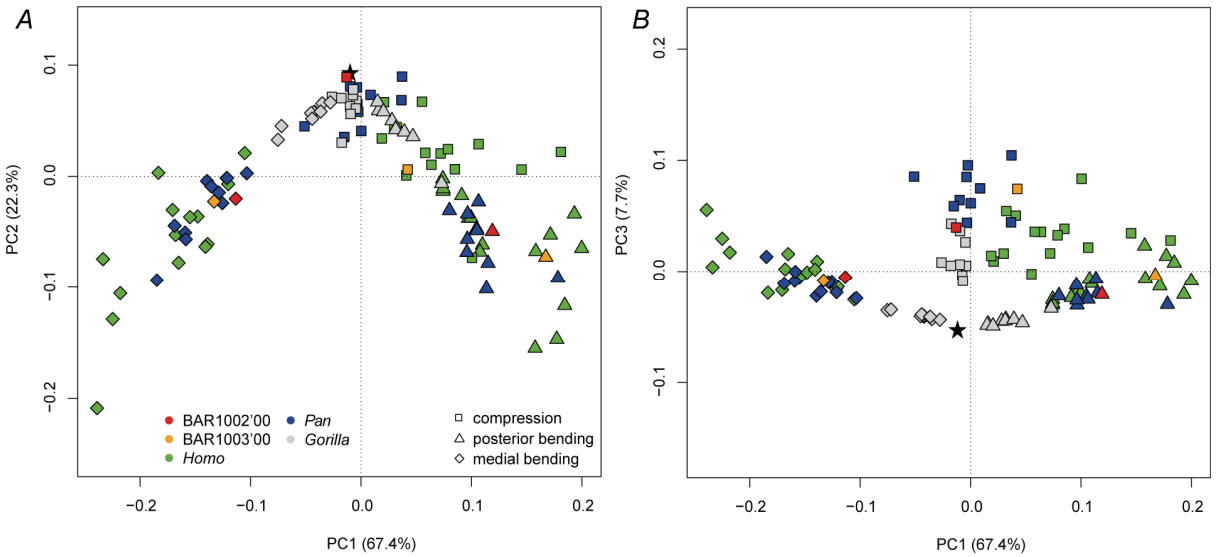

Fig. 9. PCA of the FEA results for compression, medial bending and posterior bending of BAR1002'00 and BAR1003'00 (*Orrorin*) and of three samples of extant humans (*Homo*), chimpanzees (*Pan*) and gorillas (*Gorilla*) following the first and second (*A*) and the first and third axes (*B*). The black star represents the unloaded mean specimen.

Fig. 9. PCA des résultats des FEA pour la compression et la torsion médiale et postérieure de BAR1002'00 et BAR1003'00 (*Orrorin*), ainsi que de trois échantillons actuels d'humains (*Homo*), chimpanzés (*Pan*) et gorilles (*Gorilla*) selon le premier et deuxième axe (A) et selon le premier et troisième axe (B). L'étoile noire représente la moyenne du spécimen non contraint.

The results of the analysis where all loadcases have been combined within each investigated specimen are summarized in the bivariate plot of Fig. 10. With their negative values on PC1 (73.5%), the gorillas are less deformed than the chimpanzees, but chimps are nonetheless distributed along the same vector, which is distinct from the human pattern (Fig. 10A). Following this axis, *Pan* and *Homo* overlap, but not on PC2 (12.8%). In this morphospace, BAR 1002'00 is

deformed like a chimp, while BAR 1003'00 behaves as a human femur. Instead, when PC3 is considered (3.9%), both *Orrorin* femora are closer to the African apes (Fig. 10B).

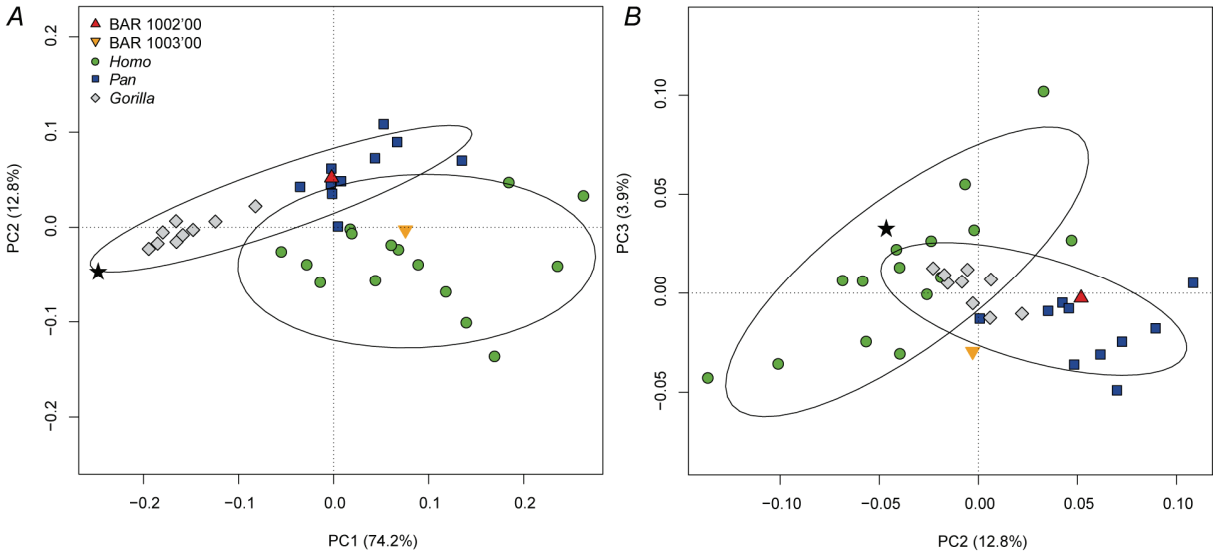

Fig. 10. PCA of the combined FEA results of BAR1002'00 and BAR1003'00 (*Orrorin*) and of three samples of extant humans (*Homo*), chimpanzees (*Pan*) and gorillas (*Gorilla*) following the first and second (A) and the second and third axes (B). The black star represents the unloaded mean specimen. The ellipse confidence interval is of 95%.

Fig. 10. PCA des résultats combinés des FEA de BAR1002'00 et BAR1003'00 (*Orrorin*), ainsi que de trois échantillons actuels d'humains (*Homo*), chimpanzés (*Pan*) et gorilles (*Gorilla*) selon le premier et deuxième axe (A) et selon le premier et troisième axe (B). L'étoile noire représente la moyenne du spécimen non contraint. L'intervalle de confiance de l'ellipse est de 95%.

References

Almécija, S., Tallman, M., Alba, D.M., Pina, M., Moyà-Solà, S., Jungers, W.L., 2013. The femur of *Orrorin tugenensis* exhibits morphometric affinities with both Miocene apes and later hominins. Nature Comm. 4:2888 (doi: 10.1038/ncomms3888).

Baddeley, A., 2008. Analyzing Spatial Point Patterns in R. www.csiro.au/resources/pf16h.html.

Bleuze, M., 2012. Proximal femoral diaphyseal cross-sectional geometry in *Orrorin tugenensis*. HOMO J. Comp. Hum. Biol. 63, 153–166.

Bondioli, L., Bayle, P., Dean, C., Mazurier, A., Puymerail, L., Ruff, C., Stock, J.T., Volpato, V., Zanolli, C., Macchiarelli, R., 2010. Morphometric maps of long bone shafts and dental roots for imaging topographic thickness variation. Am. J. Phys. Anthropol. 142, 328–334.

Bookstein, F.L., 1991. Morphometric Tools for Landmark Data: Geometry and Biology. Cambridge University Press, Cambridge.

Carlson, K.J., 2006. Muscle architecture of the common chimpanzee (*Pan troglodytes*): Perspectives for investigating chimpanzee behavior. Primates 47, 218–229.

Carter, D.R., Beaupré, G.S., 2007. Skeletal Function and Form: Mechanobiology of Skeletal Development, Aging, and Regeneration. Cambridge University Press, New York.

Coleman, M.N., Colbert, M.W., 2007. Technical note. CT thresholding protocols for taking measurements on three-dimensional models. Am. J. Phys. Anthropol. 133, 723–725.

Currey, J.D., 2002. Bones: Structure and Mechanics. Princeton University Press, Oxford.

Dryden, I.L., Mardia, K.V., 1998. Statistical Shape Analysis. Wiley, New York.

Fagan, M.J., Curtis, N., Dobson, C.A., Karunanayake, J.H., Kitpczik, K., Moazen, M., Page, L., Phillips, R., O'Higgins, P., 2007. Voxel-based finite element analysis-working directly with micro CT scan data. J. Morphol. 268, 1071.

Fajardo, R.J., Ryan, T.M., Kappelman, J., 2002. Assessing the accuracy of high-resolution X-ray computed tomography of primate trabecular bone by comparisons with histological sections. Am. J. Phys. Anthropol. 118, 1–10.

Fitton, L.C., Shi, J.F., Fagan, M.J., O'Higgins, P. 2012. Masticatory loadings and cranial deformation in *Macaca fascicularis*: A finite element analysis sensitivity study. J. Anat. 221, 55–68.

Galik, K., Senut, B., Pickford, M., Gommery, D., Treil, J., Kuperavage, A.J., Eckhardt, R.B., 2004. External and internal morphology of the BAR 1002'00 *Orrorin tugenensis* femur. Science 305, 1450–1454.

Gibbs, S., Collard, M., Wood, B., 2002. Soft-tissue anatomy of the extant hominoids: A review and phylogenetic analysis. J. Anat. 200, 3–49.

Gommery, D., Senut, B., 2006. La phalange distale du pouce d'*Orrorin tugenensis* (Miocène supérieur du Kenya). Geobios 39, 372–384.

Jensvold, M.L.A., Sanz, C.M., Fouts, R.S., Fouts, D.H., 2001. Effect of enclosure size and complexity on the behaviors of captive chimpanzees (*Pan troglodytes*). J. Appl. Anim. Welf. Sci. 4, 53–69.

Kuperavage, A.J., Eckhardt, R.B., 2009. Biomechanical inferences about the origins of bipedal locomotion from ancient African femora. J. Eng. Mech. 135, 479–484.

Kuperavage, A.J., Sommer, H.J., Eckhardt, R.B., 2010. Moment coefficients of skewness in the femoral neck cortical bone distribution of BAR 1002'00. HOMO J. Comp. Hum. Biol. 61, 244–252.

Lieberman, D.E., Polk, J.D., Demes, B., 2004. Predicting long bone loading from cross-sectional geometry. Am. J. Phys. Anthropol. 123, 156–171.

Lovejoy, C.O., Burstein, A.H., Heiple, K.G., 1976. The biomechanical analysis of bone strength: A method and its application to platycnemia. Am. J. Phys. Anthropol. 44, 489–506.

Lovejoy, C.O., Meindl, R.S., Ohman, J.C., Heile, K.G., White, T.D., 2002. The Maka femur and its bearing on the antiquity of human walking: Applying contemporary concepts of morphogenesis to the human fossil record. Am. J. Phys. Anthropol. 119, 97–88.

Lovejoy, C.O., Suwa, G., Spurlock, L., Asfaw, B., White, T.D., 2009. The pelvis and femur of *Ardipithecus ramidus*: The emergence of upright walking. Science 326, 71–76.

Marchi, D., 2005. The cross-sectional geometry of the hand and foot bones of the Hominoidea and its relationship to locomotor behavior. J. Hum. Evol. 53, 647–655.

Marchi, D., 2007. Relative strength of the tibia and fibula and locomotor behavior in hominoids. J. Hum. Evol. 49, 743–761.

Matsumura, A., Takahashi, Y., Okada, M., 2002. Cross-sectional geometric properties along the diaphysis of femur and humerus in chimpanzees and humans. Zeit. Morph. Anthropol. 83, 373–382.

Mazurier, A., Nakatsukasa, M., Macchiarelli, R., 2010. The inner structural variation of the primate tibial plateau characterized by high-resolution microtomography. Implications for the reconstruction of fossil locomotor behaviours. CR Palevol 9, 349–359.

McHenry, H., 1974. How large were the australopithecines? Am. J. Phys. Anthrop. 40, 329–340.

Milne, N., O'Higgins, P., 2012. Scaling of form and function in the xenarthran femur: A 100-fold increase in body mass is mitigated by repositioning of the third trochanter. Proc. Biol. Sci. 279, 3449–3456.

Morimoto, N., Ponce de León, M.S., Nishimura, T., Zollikofer, C.P.E., 2011b. Femoral morphology and femoropelvic musculoskeletal anatomy of humans and great apes: A comparative virtopsy study. Anat. Rec. 294, 1433–1445.

Morimoto, N., Ponce de León, M.S., Zollikofer, C.P.E., 2011a. Exploring femoral diaphyseal shape variation in wild and captive chimpanzees by means of morphometric mapping: A test of Wolff's law. Anat. Rec. 294, 589–609.

Morimoto, N., Zollikofer, C.P.E., Ponce de León, M.S., 2012. Shared human-chimpanzee pattern of perinatal femoral shaft morphology and its implications for the evolution of hominin locomotor adaptations. PLoS ONE 7, e41980.

Nakatsukasa, M., Pickford, M., Egi, N., Senut, B., 2007. Femur length, body mass, and stature estimates of *Orrorin tugenensis*, a 6 Ma hominid from Kenya. Primates 48, 171–178.

O'Higgins, P., 2000. The study of morphological variation in the hominid fossil record: Biology, landmarks and geometry. J. Anat. 197, 103–106.

O'Higgins, P., Cobb, S.N., Fitton, L.C., Gröning, F., Phillips, R., Liu, J., Fagan, M.J., 2011. Combining geometric morphometrics and functional simulation: An emerging toolkit for virtual functional analyses. J. Anat. 218, 3–15.

O'Higgins, Fitton, L.C., Phillips, R., Shi, J.F., Liu, J., Gröning, F., Cobb, S.N., Fagan, M.J., 2012. Virtual functional morphology: Novel approaches to the study of craniofacial form and function. Evol. Biol. 59, 521–535.

O'Higgins, P., Jones, N., 2006. Morphologika², Tools for Shape Analysis Computer Software. University College London, London (http://www.york.ac.uk/res/fme/resources/software.htm).

Ohman, J.C., Krochta, T.J., Lovejoy, C.O., Mensforth, R.P., Latimer, B., 1997. Cortical bone distribution in the femoral neck of hominoids: Implications for the locomotion of *Australopithecus afarensis*. Am. J. Phys. Anthropol. 104, 117–131.

Oxnard, C., O'Higgins, P., 2009. Biology clearly needs morphometrics. Does morphometrics need biology? Biol. Theory 4, 84–97.

Pebesma, E.J., 2004. Multivariable geostatistics in S: The gstat package. Comp. Geosc. 30, 683–691.

Pickford, M., Senut, B., Gommery, D., Treil, J., 2002. Bipedalism in *Orrorin tugenensis* revealed by its femora. C.R. Palevol 1,191–203.

Puymerail, L., 2011. Caractérisation de l'Endostructure et des Propriétés Biomécaniques de la Diaphyse fémorale: la Signature de la Bipédie et la Reconstruction des Paléo-Répertoires Posturaux et Locomoteurs des Hominines. Ph.D. dissertation. Muséum national d'Histoire naturelle, Paris.

Puymerail, L., 2013. The functionally-related signatures characterizing the endostructural organisation of the femoral shaft in modern humans and chimpanzee. C.R. Palevol 12, 223–231.

Puymerail, L., O'Higgins, P., 2013. Reading function from long bones: Implications for the reconstruction of early hominin postural and locomotor behaviours. 3rd Annual Meeting of the European Society for the Study of Human Evolution (Vienna, 20–21/9/2013), abstract, p. 156.

Puymerail, L., Ruff, C.B., Bondioli, L., Widianto, H., Trinkaus, E., Macchiarelli, R., 2012. Structural analysis of the Kresna 11 *Homo erectus* femoral shaft (Sangiran, Java). J. Hum. Evol. 63, 741–749.

R Development Core Team, 2013. R: A Language and Environment for Statistical Computing. R Foundation for Statistical Computing, Vienna (http://www.R-project.org).

Rasband, W.S., 2010. ImageJ. US National Institutes of Health. Bethesda, Maryland (http://rsb.info.nih.gov/ij/).

Reilly, D.T., Burstein, A.H., 1975. The elastic and ultimate properties of compact bone tissue. J. Biomech. 8, 393–405.

Richmond, B.G., Jungers, W.L., 2008. *Orrorin tugenensis* femoral morphology and the evolution of hominin bipedalism. Science 319, 1662–1665.

Richmond, B.G., Jungers, W.L., 2012. Hominin proximal femur morphology from the Tugen Hills to Flores. In Reynolds, S.C., Gallagher, A. (Eds.), African Genesis: Perspectives on Hominin Evolution. Cambridge University Press, Cambridge, pp 248–267.

Ruff, C.B., 2008. Biomechanical analyses of archaeological human skeletal samples. In Katzenberg, M.A., Saunders, S.R. (Eds.), Biological Anthropology of the Human Skeleton. Wiley-Liss, Hoboken, pp. 183–206.

Ruff, C.B., Hayes, W.C., 1983. Cross-sectional geometry of Pecos Pueblo femora and tibiae - a biomechanical investigation. I. Method and general patterns of variation. Am. J. Phys. Anthropol. 60, 359–381.

Ruff, C.B., Higgins, R., 2013. Femoral neck structure and function in early hominins. Am. J. Phys. Anthropol. 150, 512–525.

Ruff, C.B., Holt, B., Trinkaus, E., 2006. Who's afraid of the big bad Wolff?: "Wolff's Law" and bone functional adaptation. Am. J. Phys. Anthropol. 129, 484–498.

Ruff, C.B., McHenry, H.M., Thackeray, J.F., 1999. Cross-sectional morphology of the SK 82 and 97 proximal femora. Am. J. Phys. Anthropol. 109, 509–521.

Sawada, Y., Pickford, M., Senut, B., Itaya, T., Hyodo, M., Miura, M., Kashine, C., Chujo, T., Fujii, H., 2002. The age of *Orrorin tugenensis*, an early hominid from the Tugen Hills, Kenya. C.R. Palevol 1, 293–303.

Senut, B., 2006. Bipédie et climat. C.R. Palevol 5, 89–98.

Senut, B., Pickford, M., Gommery, D., Mein, P., Cheboi, K., Coppens, Y., 2001. First hominid from the Miocene (Lukeino Formation, Kenya). C.R. Acad. Sci. Paris, Ser.IIa 332, 137–144.

Sigmon, B.A., 1974. A functional analysis of pongid hip and thigh musculature. J. Hum. Evol. 3, 161–185.

Slice, D.E., 2005. Modern Morphometrics in Physical Anthropology. University of Chicago, Chicago.

Spoor, F., Zonneveld, F., Macho, G.A., 1993. Linear measurements of cortical bone and dental enamel by computed tomography: Applications and problems. Am. J. Phys. Anthropol. 91, 469–484.

Swindler, D.R., Wood, C.D., 1973. An Atlas of Primate Gross Anatomy: Baboon, Chimpanzee, and Man. University of Washington Press, Seattle.

Thorpe, S.K.S., Holder, R.L., Crompton, R.H., 2007. Origin of human bipedalism as an adaptation for locomotion on flexible branches. Science 316, 1328–1331.

Viceconti, M., Ansaloni, M., Baleani, M., Toni, A., 2003. The muscle standardized femur: A step forward in the replication of numerical studies in biomechanics. Proc. Inst. Mech. Eng. H 217, 105–110.

Wood, S.N., 2006. Generalized Additive Models: An Introduction with R. Chapman & Hall, Boca Raton.

Wood, B., Harrison, T., 2011. The evolutionary context of the first hominins. Nature 470, 347–352.

Zebaze, R.M.D., Jones, A., Knackstedt, M., Maalouf, G., Seeman, E., 2007. Construction of the femoral neck during growth determines its strength in old age. J. Bone Min. Res. 22, 1055–1061.

Zebaze, R.M.D., Jones, A., Welsh, F., Knackstedt, M., Seeman, E. 2005. Femoral neck shape and the spatial distribution of its mineral mass varies with its size: Clinical and biomechanical implications. Bone 37, 234–252.

Zollikofer, C.P.E., Ponce de León, M.S., 2001. Computer-assisted morphometry of hominoid fossils: the role of morphometric maps. In de Bonis, L., Koufos, G.D., Andrews, P. (Eds.), Hominoid Evolution and Climate Change in Europe. Phylogeny of the Neogene Hominoid Primates of Eurasia. Cambridge University Press, Cambridge, pp 50–59.